Nonlocal Interactions in Moiré Hubbard Systems

Nicolás Morales-Durán,[1,*] Nai Chao Hu,[1] Pawel Potasz,[2] and Allan H. MacDonald[1]
[1]Department of Physics, University of Texas at Austin, Austin, Texas 78712, USA
[2]Institute of Physics, Faculty of Physics, Astronomy and Informatics, Nicolaus Copernicus University, Grudziadzka 5, 87-100 Toruń, Poland

(Received 16 August 2021; revised 19 January 2022; accepted 2 May 2022; published 24 May 2022)

Moiré materials formed in two-dimensional semiconductor heterobilayers are quantum simulators of Hubbard-like physics with unprecedented electron density and interaction strength tunability. Compared to atomic scale Hubbard-like systems, electrons or holes in moiré materials are less strongly attracted to their effective lattice sites because these are defined by finite-depth potential extrema. As a consequence, nonlocal interaction terms like interaction-assisted hopping and intersite exchange are more relevant. We theoretically demonstrate the possibility of tuning the strength of these coupling constants to favor unusual states of matter, including spin liquids, insulating ferromagnets, and superconductors.

DOI: 10.1103/PhysRevLett.128.217202

Introduction.—Moiré materials have emerged as an attractive controllable platform to simulate and explore quantum condensed matter [1–6]. The electronic structure of moiré materials is accurately described by continuum models with moiré spatial periodicity that can be engineered to yield Bloch bands with controllable width [3] and topology [7,8]. For moiré bilayers formed by transition metal dichalcogenides (TMD), electrons in the valence moiré band can experience triangular or honeycomb lattice symmetry periodic potentials, depending on the TMD monolayer constituents, and the closest commensurate stacking arrangement. For small twist angles the low-energy physics can correspondingly be described by either a single-band or a two-band model with a locked spin-valley pseudospin [3–6]. The emergent many-body physics, which is extremely sensitive to the flat-band filling factor $\nu = N/N_M$, can be modeled theoretically by adding electronic interactions to the continuum band model directly in momentum space [6,9] or by mapping the minibands to generalized Hubbard models. (Here, N is the number of electrons or holes and N_M is the number of moiré periods in the system.) Recent experiments in moiré TMD homobilayers and heterobilayers have exploited the possibility of tuning ν through large ranges with electrical gates, discovering Mott [10,11] and quantum anomalous Hall [12] insulating states at $\nu = 1$ and generalized Wigner crystal states at several rational fractional fillings [13–15]. The appearance of Wigner crystal states establishes the importance of long-range interactions in the many-body physics of semiconductor moiré materials, which are expected to enrich phase diagrams [9].

In this Letter, we show that off-diagonal in-site interactions, often ignored in studies of Hubbard model physics, play a significant role in determining the ground state properties of semiconductor moiré materials. Starting from continuum model Bloch states, we use a projection technique [16–18] to obtain Wannier functions of holes localized on moiré superlattice sites. From these Wannier functions we calculate generalized Hubbard model parameters, that we use to derive a low-energy spin model description valid for strong interaction strengths at $\nu = 1$. For small twist angles, or equivalently large moiré lattice constants, the Wannier orbitals are well approximated by the eigenstates of a harmonic potential and therefore an on-site Hubbard model description is justified. Decreases in the moiré lattice constant or the modulation potential strength lead to overlaps between the tails of Wannier functions localized on nearest-neighbor lattice sites (see Supplemental Material [19]). When significant, the overlap gives rise to enhanced nonlocal interaction terms. In exploring their influence, we have focused on the spin physics of Mott insulator states at $\nu = 1$. Our main results are presented in Fig. 1. In Figs. 1(a) and 1(b) we show Heisenberg model spin coupling constants for a small twist angle with well-localized Wannier orbitals, and for a larger twist angle with significant Wannier function overlap between neighbors. As illustrated in 1(c), we find that the nearest-neighbor interaction J_1 changes sign as a function of twist angle and background dielectric screening, indicating the possibility of controlled tuning between antiferromagnetic and ferromagnetic states. We confirm this transition by finite size exact diagonalization calculations. Hartree-Fock analyses of heterobilayers [20,21] and homobilayers [8,22] have also identified a ferromagnetic phase as a candidate ground state at $\nu = 1$ when dielectric screening is weak. For larger twist angles, which are more relevant experimentally, contributions of other two- and four-spin terms become important in spin model descriptions of TMD moiré materials. Our findings suggest strategies to create unusual states, including ferromagnetic insulators, spin liquids, and superconductors.

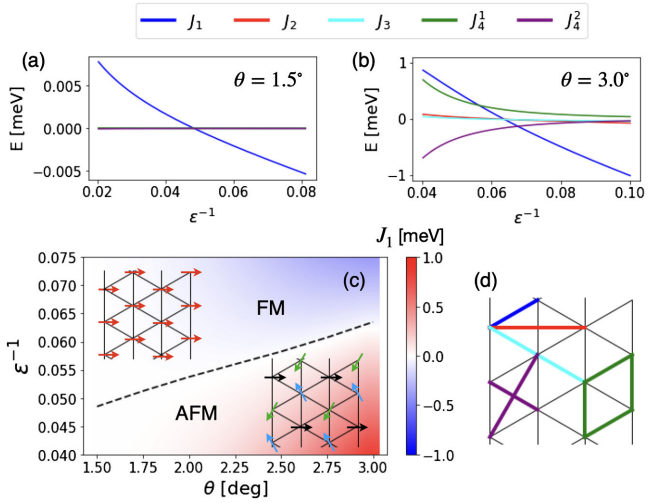

FIG. 1. Spin model coupling constants of the Mott insulator state at $\nu = 1$ for a heterobilayer at small twist angle (long moiré length) (a) and at a larger twist angle (shorter moiré length) (b), as a function of interaction strength ϵ^{-1}. (c) Phase diagram of a $\nu = 1$ twisted heterobilayer vs interaction strength ϵ^{-1} and twist angle θ, indicating the antiferromagnet-ferromagnet transition line. Color scale shows the magnitude of the first-neighbor Heisenberg coupling J_1. (d) Schematic illustrations of the neighbor configuration for the various coupling constants presented in the upper panels (a) and (b). These calculations were performed for a modulation potential with $\psi = -94°$ and $V_m = 11$ meV (see main text).

Generalized Hubbard model for moiré TMDs.—We limit our attention to TMD heterobilayers that form triangular moiré superlattices and therefore permit a single-band low-energy description with trivial topology. Assuming a smooth potential limit [3], the continuum model that describes the bilayer's electronic structure depends only on the moiré lattice constant a_M, the modulation potential strength V_m, and a single potential-shape parameter ψ (for details on the continuum model see Supplemental Material [19]). The continuum model can be mapped to a real space lattice model, whose Hamiltonian is written in the most general way as

$$H = -\sum_{i,j,\sigma} t_{ij} c^\dagger_{i,\sigma} c_{j,\sigma} + \frac{1}{2} \sum_{\substack{i,j,k,l \\ \sigma\sigma'}} V^{\sigma,\sigma'}_{ijkl} c^\dagger_{i,\sigma} c^\dagger_{j,\sigma'} c_{l,\sigma'} c_{k,\sigma}, \quad (1)$$

where $c^\dagger_{i,\sigma}(c_{i,\sigma})$ creates (destroys) an electron at site i in valley σ; i, j, k, and l are site labels, t_{ij} stands for the hopping integral between sites i and j, and $V^{\sigma\sigma'}_{ijkl}$ is a two-particle matrix element

$$V^{\sigma,\sigma'}_{i,j,k,l} = \langle \mathbf{R}_i, \mathbf{R}_j | V | \mathbf{R}_k, \mathbf{R}_l \rangle, \quad (2)$$

with $\mathbf{R}_i$ the moiré lattice site positions. The Coulomb long-range interaction is given by $V = e^2/\epsilon|\mathbf{r}_1 - \mathbf{r}_2|$ and ϵ^{-1} is the system's dielectric screening from the surrounding environment, which determines the interaction strength. Since $V^{\sigma,\sigma'}_{i,j,k,l}$ is invariant under global translations, we can choose $\mathbf{R}_i = 0$. The largest matrix elements are the on-site interactions $U_0 = \langle \mathbf{0}, \mathbf{0} | V | \mathbf{0}, \mathbf{0} \rangle$, and two-center integrals involving sites 0 and $\mathbf{R}$. The latter include the nearest-neighbor direct interaction $U_1 = \langle \mathbf{0}, \mathbf{R} | V | \mathbf{0}, \mathbf{R} \rangle$, intersite-exchange $X_1 = \langle \mathbf{0}, \mathbf{R} | V | \mathbf{R}, \mathbf{0} \rangle$, assisted hopping $A_1 = \langle \mathbf{0}, \mathbf{0} | V | \mathbf{0}, \mathbf{R} \rangle$, and pair-hopping $P_1 = \langle \mathbf{0}, \mathbf{0} | V | \mathbf{R}, \mathbf{R} \rangle$ matrix elements.

For single-particle potentials that are strongly attractive on lattice sites, like those of atomic-scale ionic crystals, Wannier functions are well localized, and nonlocal interactions that require overlap between distinct Wannier functions are usually negligible. In the intermediate case of d-band electrons in an elemental transition metal crystal Hubbard estimated that $U_0 \sim 20$ eV, $U_1 \sim 6$ eV, $A \sim 0.5$ eV, and X, $P \sim 1/40$ eV [23]. Because nearest-neighbor interaction terms can be reduced by screening, it is sometimes justified to retain only U_0, yielding the standard on-site Hubbard model. In general, a less attractive potential has more extended Wannier functions, modifying the relationship between the various interaction terms. Nonlocal interactions have been considered previously in extended Hubbard model theories of polyacetylene [24–26], where they enhance dimerization, and can produce a ferromagnetic phase but only in parameter ranges that appear to be unphysical. Because the assisted hopping interaction may acquire a large multiplicative factor related to lattice geometry, it can play a significant role even when much smaller than U_0, potentially causing pairing and leading to superconductivity [27,28]. In the following, we address the importance of nonlocal terms in twisted TMD heterobilayers, concentrating on their role in determining $\nu = 1$ ground state properties.

From eigenvectors and eigenvalues of the continuum model's topmost band we obtain Wannier functions localized at moiré lattice sites and evaluate extended Hubbard model parameters $t_{i,j}$ and $V_{i,j,k,l}$, shown as lines with dots in Fig. 2, as described in [19]. As a consistency check, we compare our extended Hubbard model parameters with the ones obtained in the regime of large a_M, where the modulation potential minima can be approximated by a set of harmonic potentials centered on moiré lattice sites [3] and analytic control is possible. In this limit, the Wannier functions are

$$\psi_{\mathbf{R}}(\mathbf{r}) = \left(\frac{1}{\pi a_W^2}\right)^{1/2} \exp\left[-\frac{(\mathbf{r} - \mathbf{R})^2}{2a_W^2}\right], \quad (3)$$

where $a_W = \kappa^{1/4}\sqrt{a_M}$ is the Wannier function width and $\kappa = \hbar^2/[16\pi^2 V_m m^* \cos(120° + \psi)]$ varies inversely with modulation potential strength. In this approximation $a_M \sim a_0/\theta$, with a_0 the active layer's lattice constant. We find that the near-neighbor hopping amplitude is

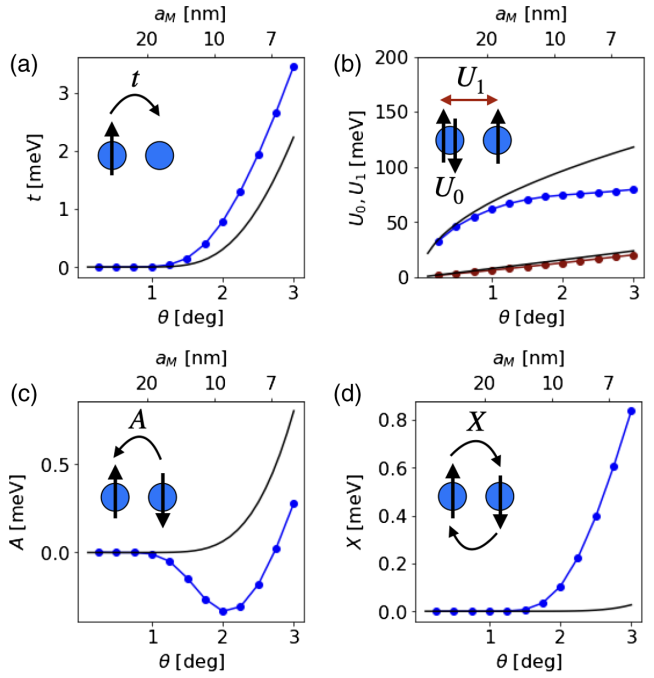

FIG. 2. Comparison between harmonic approximation (solid black lines) and exact continuum model results (lines with dots) for (a) hopping, (b) on-site (blue) and first-neighbor (dark red) interactions, (c) assisted hopping, and (d) intersite exchange interactions. Interaction parameters are plotted vs twist angle (bottom axes) and vs moiré length (top axes). The insets provide schematic illustrations of each process. These calculations are for $V_m = 11$ meV, $\psi = -94°$, and $\epsilon = 10$.

$$t = \frac{\hbar^2}{2m^* a_W^2}\left(\frac{a_M^2}{4a_W^2} - 1\right)\exp\left[-\frac{a_M^2}{4a_W^2}\right] = \frac{\hbar^2}{2m^*\kappa^{1/2}}\left(\frac{1}{4\kappa^{1/2}} - \frac{\theta}{a_0}\right)\exp\left[-\frac{a_0}{4\kappa^{1/2}\theta}\right], \quad (4)$$

while the most significant interaction matrix elements are

$$U_0 = \frac{\pi^{1/2}e^2}{\sqrt{2}\epsilon a_W} \sim \sqrt{\theta}, \quad (5)$$

$$U_1 = \frac{2e^2 I_1}{\sqrt{\pi}\epsilon a_W} \sim \sqrt{\theta} I_1, \quad (6)$$

$$A_1 = \frac{I_2}{I_1} U_1 \exp\left[-\frac{a_M^2}{4a_W^2}\right] \sim \sqrt{\theta} I_2 \exp\left[-\frac{a_0}{4\kappa^{1/2}\theta}\right], \quad (7)$$

$$X_1 = P_1 = U_0 \exp\left[-\frac{a_M^2}{2a_W^2}\right] \sim \sqrt{\theta}\exp\left[-\frac{a_0}{2\kappa^{1/2}\theta}\right], \quad (8)$$

with I_1 and I_2 integrals given in Supplemental Material [19].

A comparison between the analytical expressions given by Eqs. (4)–(8) and the results for extended Hubbard model parameters obtained from numerical calculations as a function of twist angle is provided in Fig. 2. For small twist angles we see good agreement, as expected, while for larger twist angles the harmonic approximation underestimates Wannier function tails, and therefore nonlocal interaction strengths. Interestingly, we see in Fig. 2(c) that the nonlocal exchange interaction X_1 increases significantly with twist angle, and in Fig. 2(d) that there is a range of angles for which the assisted hopping amplitude A_1 becomes negative. These qualitative differences between the harmonic potential approximation and exact results are expected since the lattice potentials in the former model have unbounded strength, whereas the actual potential is bounded, causing that for $\theta \gtrsim 2.0°$ the Wannier functions are more extended and acquire negative tails [19].

Effective spin model.—To illustrate the qualitative impact of nonlocal interactions on moiré Hubbard physics, we focus on the spin physics of the Mott insulator states at $\nu = 1$. The charge gap of the Mott insulators is set by the U_0 energy scale that makes double occupancy of any lattice site energetically unfavorable. When U_0 is larger than all other energy scales, the Hubbard spectrum separates into two branches, an upper branch with a large double occupation weight, and a low-energy branch in which charge is approximately frozen and is described by a spin Hamiltonian

$$H_{\text{eff}} = J_1 \sum_{\langle i,j\rangle} \mathbf{S}_i \cdot \mathbf{S}_j + J_2 \sum_{\langle\langle i,j\rangle\rangle} \mathbf{S}_i \cdot \mathbf{S}_j + J_3 \sum_{\langle\langle\langle i,j\rangle\rangle\rangle} \mathbf{S}_i \cdot \mathbf{S}_j + \sum_{\square} J_4^1[(\mathbf{S}_i \cdot \mathbf{S}_j)(\mathbf{S}_k \cdot \mathbf{S}_l) + (\mathbf{S}_i \cdot \mathbf{S}_l)(\mathbf{S}_j \cdot \mathbf{S}_k)] + J_4^2(\mathbf{S}_i \cdot \mathbf{S}_k)(\mathbf{S}_j \cdot \mathbf{S}_l), \quad (9)$$

where the $\mathbf{S}_i$ are spin operators and the summations are over first nearest neighbors, second nearest neighbors, third nearest neighbors, and ring clusters, respectively. The coupling constants of the spin model can be expressed in terms of the real space Coulomb matrix elements by applying a cluster perturbation expansion [29] or equivalently a Schrieffer-Wolff transformation [30] to the Hamiltonian in Eq. (1), as detailed in Supplemental Material [19]. We show that the dominant near-neighbor coupling constant $J_1 \approx 4(t_1 - A_1)^2/(U_0 - U_1) - 2X_1$ has independent contributions from two different mechanisms, an antiferromagnetic superexchange contribution that is inversely proportional to interaction strength, and a ferromagnetic direct exchange contribution that is proportional to interaction strength. Because the two contributions respond oppositely to changes in interaction strength, the one that dominates can be changed by controlling the dielectric constant ϵ of the surrounding material. Typical results for the dependence of spin-model coupling constants on ϵ^{-1} are shown in Figs. 1(a) and 1(b) for angles $\theta = 1.5°$ and $\theta = 3.0°$, respectively.

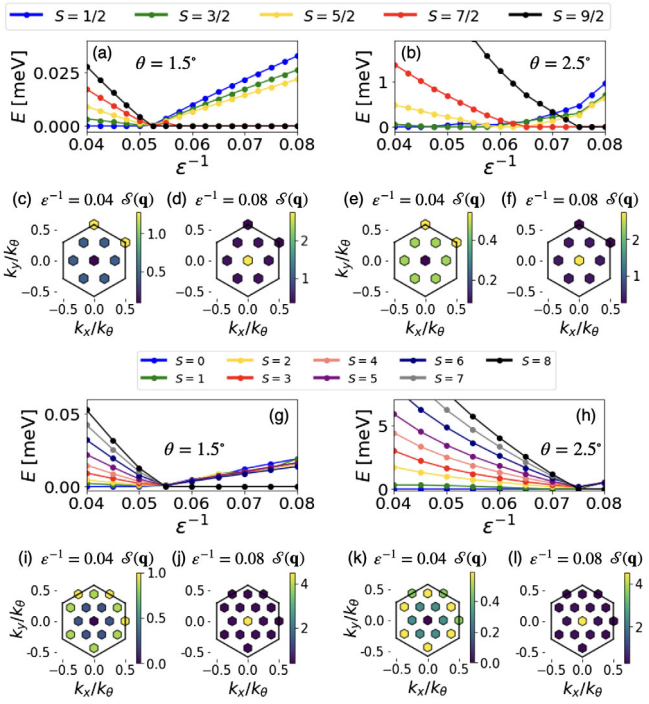

FIG. 3. Transition from antiferromagnet to ferromagnet as seen by exact diagonalization of the continuum model. The evolution of the lower Hubbard band vs ϵ^{-1} for (a) $\theta = 1.5°$ and (b) $\theta = 2.5°$. Evolution of the lowest energy state for each S vs ϵ^{-1} for (c) $\theta = 1.5°$ and (d) $\theta = 2.5°$. Spin structure factors for twist angle $\theta = 1.5°$ in the antiferromagnetic (e) and ferromagnetic (f) phases and for twist angle $\theta = 2.5°$ in the antiferromagnetic (g) and ferromagnetic (h) phases. Axes in structure factor plots are normalized by $k_\theta = 4\pi/\sqrt{3}a_M$, the length of the moiré reciprocal lattice vectors.

In Fig. 1(a) we see that for small angles or long moiré periods, J_1 is the dominant coupling constant. The many-body ground state of the system is expected to be antiferromagnetic for $J_1 > 0$ and ferromagnetic for $J_1 < 0$. To demonstrate this behavior explicitly, we calculate the full low-energy spectrum of the TMD bilayer by finite-size exact diagonalization of the continuum model. Performing ED directly in momentum space allows us to include all long-range interactions. The evolution of the lowest eigenvalue with total spin quantum number S for $\theta = 1.5°$ and $\theta = 2.5°$, with respect to ϵ^{-1}, is plotted in Figs. 3(a) and 3(b) for $N = 9$ and in Figs. 3(g) and 3(h) for $N = 16$. From these results we see that for the smaller angle the ground state is a singlet when $J_1 > 0$, as expected for an antiferromagnetic state and that for the region where $J_1 < 0$ the ground state is a ferromagnet. The spin structure factors calculated in the antiferromagnetic phase, shown in Figs. 3(c) and 3(i), show peaks at the corners of the Brillouin zone, indicating a three-sublattice state, while the structure factors in the ferromagnetic phase, shown in Figs. 3(d) and 3(j), have a peak at γ, characteristic of a ferromagnetic state. At larger twist angles the harmonic approximation is not accurate and nearest-neighbor coupling J_1 is less dominant. In this case we also have a ferromagnetic insulating ground state for large ϵ^{-1} and an antiferromagnetic ground state for small ϵ^{-1} for both system sizes, as can be seen from total spin S plots, Figs. 3(b) and 3(h) and structure factors, Figs. 3(e), 3(f), 3(k), and 3(l). The region near where J_1 changes sign is now more complex, as can be observed from our finite-size calculations. Although our ED calculations cannot determine the thermodynamic limit ground state in this regime, it is clear that exotic spin states are likely to be abundant close to the antiferromagnet-ferromagnet transition. Ring-exchange terms J_4^1 and J_4^2 become significant and may favor spin liquid ground states [31,32] and the contributions from J_2 and J_3 also suggest exotic spin states. In Fig. 1(b), as interaction strength ϵ^{-1} increases, the superexchange couplings J_3, J_2, J_1 change sign from positive to negative sequentially. In the region where $J_3 < 0$ but $J_1 > J_2 \gtrsim 0$, there is bound to be a point where $-J_1/J_3 = 9$. Close to that point, another antiferromagnetic spin configuration, the stripe state [20,33], has a very similar classical energy to the three-sublattice state, making quantum fluctuations important in determining the ground state.

Discussion.—We have shown that nonlocal interaction terms can be sizable in semiconductor moiré materials and that they can have an important influence on electronic properties, giving rise to moiré Mott-Hubbard ferromagnets, not expected in other systems described by Hubbard models with only local interaction terms. Nonlocal interactions become more prominent at larger twist angles and at weaker moiré modulation, where a harmonic expansion of the modulation potential near its minima fails to describe the band Wannier functions (see Fig. 2), justifying the methodology employed here. In the case of the Mott insulator states that appear at moiré filling factor $\nu = 1$, nonlocal exchange supplies a ferromagnetic contribution to the near-neighbor interaction between spins that is comparable in strength to the antiferromagnetic superexchange contribution, making sign changes in the total interaction common over typical ranges of experimental parameters. In particular, current WSe_2/WS_2 samples with $a_M \sim 8$ nm [11,13–15] appear on the antiferromagnetic side of the phase boundary and the competition with ferromagnetism can be tuned *in situ* by varying the moiré modulation strength, which mainly influences t_1—using gate electric fields [34,35] or pressure [36,37]—or background screening of electronic interactions, providing a promising framework to confirm the phase transition in the future. Our findings establish a strategy for engineering strongly frustrated spin-Hamiltonians that are likely to host exotic spin states.

In our explicit calculations we have considered only the case of wave vector and frequency independent background screening of the type produced by a thick surrounding dielectric, but more general situations are also relevant.

(We have focused on a range of ϵ^{-1} values that is smaller than what would be produced by screening by a surrounding h-BN dielectric alone ($\epsilon^{-1} \sim 0.2$), in anticipation of additional screening by conducting gates and by virtual transitions between flat and energetically remote moiré minibands). Similar conclusions apply to more complex moiré material states. For example, it has been established experimentally that non-near-neighbor local interaction terms U_n are important in moiré TMD systems, and that they give rise to insulating Wigner crystal states at many fractional values of ν [13–15] (presumably these Wigner crystal states would also appear in real crystals if it were possible to change the electron density without introducing disorder). The generalized Wigner crystal states also have low-energy spin sectors whose interactions are more complex than those of the $\nu = 1$ case considered here but will have coupling constants that are tunable in sign due to the competition between direct and superexchange spin interactions, determining their magnetic properties. Separately, in honeycomb lattice moiré materials [7,8,12,21,38] spin physics can be entangled with topologically nontrivial band mixing, adding another wrinkle to the low-energy physics, opening the possibility of realizing fractional Chern insulators. Finally, we remark that we have focused here on the near-neighbor exchange nonlocal interaction because it is particularly important at $\nu = 1$. Other nonlocal interactions may play a more prominent role at metallic filling factors. For example, it has been proposed [27,39] that assisted hopping can trigger superconductivity. All these issues deserve attention in future work.

The authors acknowledge helpful interactions with Kin Fai Mak and Jie Shan. We also thank Johannes Motruk for a careful examination of the spin model expressions. We acknowledge the Texas Advanced Computing Center (TACC) at The University of Texas at Austin for providing high-performance computer resources. P. P. acknowledges support from the Polish National Science Centre based on Decision No. 2021/41/B/ST3/03322. This work was supported by the U.S. Department of Energy, Office of Science, Basic Energy Sciences, under Award No. DE-SC0022106.

*Corresponding author.
na.morales92@utexas.edu

[1] E. Y. Andrei, D. K. Efetov, P. Jarillo-Herrero, A. H. MacDonald, K. F. Mak, T. Senthil, E. Tutuc, A. Yazdani, and A. F. Young, Nat. Rev. Mater. **6**, 201 (2021).
[2] D. M. Kennes, M. Claassen, L. Xian, A. Georges, A. J. Millis, J. Hone, C. R. Dean, D. N. Basov, A. N. Pasupathy, and A. Rubio, Nat. Phys. **17**, 155 (2021).
[3] F. Wu, T. Lovorn, E. Tutuc, and A. H. MacDonald, Phys. Rev. Lett. **121**, 026402 (2018).
[4] Y. Zhang, N. F. Q. Yuan, and L. Fu, Phys. Rev. B **102**, 201115(R) (2020).
[5] M. Angeli and A. H. MacDonald, Proc. Natl. Acad. Sci. U.S.A. **118**, e2021826118 (2021).
[6] N. Morales-Durán, A. H. MacDonald, and P. Potasz, Phys. Rev. B **103**, L241110 (2021).
[7] F. Wu, T. Lovorn, E. Tutuc, I. Martin, and A. H. MacDonald, Phys. Rev. Lett. **122**, 086402 (2019).
[8] H. Pan, F. Wu, and S. Das Sarma, Phys. Rev. Research **2**, 033087 (2020).
[9] H. Pan, F. Wu, and S. Das Sarma, Phys. Rev. B **102**, 201104 (R) (2020).
[10] Y. Tang, L. Li, T. Li, Y. Xu, S. Liu, K. Barmak, K. Watanabe, T. Taniguchi, A. H. MacDonald, J. Shan, and K. F. Mak, Nature (London) **579**, 353 (2020).
[11] E. C. Regan, D. Wang, C. Jin, M. I. Bakti Utama, B. Gao, X. Wei, S. Zhao, W. Zhao, Z. Zhang, K. Yumigeta, M. Blei, J. D. Carlström, K. Watanabe, T. Taniguchi, S. Tongay, M. Crommie, A. Zettl, and F. Wang, Nature (London) **579**, 359 (2020).
[12] T. Li, S. Jiang, B. Shen, Y. Zhang, L. Li, Z. Tao, T. Devakul, K. Watanabe, T. Taniguchi, L. Fu, J. Shan, and K. F. Mak, Nature (London) **600**, 641 (2021).
[13] Y. Xu, S. Liu, D. A. Rhodes, K. Watanabe, T. Taniguchi, J. Hone, V. Elser, K. F. Mak, and J. Shan, Nature (London) **587**, 214 (2020).
[14] C. Jin, Z. Tao, T. Li, Y. Xu, Y. Tang, J. Zhu, S. Liu, K. Watanabe, T. Taniguchi, J. C. Hone, L. Fu, J. Shan, and K. F. Mak, Nat. Mater. **20**, 940 (2021).
[15] X. Huang, T. Wang, S. Miao, C. Wang, Z. Li, Z. Lian, T. Taniguchi, K. Watanabe, S. Okamoto, D. Xiao, S.-F. Shi, and Y.-T. Cui, Nat. Phys. **17**, 715 (2021).
[16] J. D. Cloizeaux, Phys. Rev. **135**, A685 (1964).
[17] J. D. Cloizeaux, Phys. Rev. **135**, A698 (1964).
[18] N. Marzari and D. Vanderbilt, Phys. Rev. B **56**, 12847 (1997).
[19] See Supplemental Material at http://link.aps.org/supplemental/10.1103/PhysRevLett.128.217202 for (a) a description of the continuum model; (b) details on exact diagonalization calculations; (c) extrapolation to the thermodynamic limit of Coulomb elements; (d) expressions for the functions I_1 and I_2; (e) dependence of the results on V_m; and (f) expressions for the couplings of the effective spin model.
[20] N. C. Hu and A. H. MacDonald, Phys. Rev. B **104**, 214403 (2021).
[21] Y.-M. Xie, C.-P. Zhang, J.-X. Hu, K. F. Mak, and K. T. Law, Phys. Rev. Lett. **128**, 026402 (2022).
[22] J. Zang, J. Wang, J. Cano, and A. J. Millis, Phys. Rev. B **104**, 075150 (2021).
[23] J. Hubbard, Proc. R. Soc. A **276**, 238 (1963).
[24] S. Kivelson, W.-P. Su, J. R. Schrieffer, and A. J. Heeger, Phys. Rev. Lett. **58**, 1899 (1987).
[25] D. K. Campbell, J. T. Gammel, and E. Y. Loh, Phys. Rev. B **38**, 12043 (1988).
[26] D. K. Campbell, J. T. Gammel, and E. Y. Loh, Phys. Rev. B **42**, 475 (1990).
[27] J. E. Hirsch and F. Marsiglio, Phys. Rev. B **39**, 11515 (1989).
[28] J. E. Hirsch, Phys. Rev. B **48**, 3327 (1993).
[29] D. Antoniou and A. H. MacDonald, Phys. Rev. B **53**, 6855 (1996).
[30] A. H. MacDonald, S. M. Girvin, and D. Yoshioka, Phys. Rev. B **37**, 9753 (1988).

[31] A. Szasz, J. Motruk, M. P. Zaletel, and J. E. Moore, Phys. Rev. X **10**, 021042 (2020).
[32] T. Cookmeyer, J. Motruk, and J. E. Moore, Phys. Rev. Lett. **127**, 087201 (2021).
[33] T. Jolicoeur, E. Dagotto, E. Gagliano, and S. Bacci, Phys. Rev. B **42**, 4800 (1990).
[34] T. Li, S. Jiang, L. Li, Y. Zhang, K. Kang, J. Zhu, K. Watanabe, T. Taniguchi, D. Chowdhury, L. Fu, J. Shan, and K. F. Mak, Nature (London) **597**, 350 (2021).
[35] A. Ghiotto, E.-M. Shih, G. S. S. G. Pereira, D. A. Rhodes, B. Kim, J. Zang, A. J. Millis, K. Watanabe, T. Taniguchi, J. C. Hone, L. Wang, C. R. Dean, and A. N. Pasupathy, Nature (London) **597**, 345 (2021).
[36] M. Yankowitz, S. Chen, H. Polshyn, Y. Zhang, K. Watanabe, T. Taniguchi, D. Graf, A. F. Young, and C. R. Dean, Science **363**, 1059 (2019).
[37] M. Yankowitz, J. Jung, E. Laksono, N. Leconte, B. L. Chittari, K. Watanabe, T. Taniguchi, S. Adam, D. Graf, and C. R. Dean, Nature (London) **557**, 404 (2018).
[38] B. Andrews and A. Soluyanov, Phys. Rev. B **101**, 235312 (2020).
[39] C. Valentin and F. Liang, Sci. Adv. **7**, eabh2233 (2021).